Effective one-dimensional square well for two-dimensional quantum wires

Hua Wu and D. W. L. Sprung
Department of Physics and Astronomy, McMaster University, Hamilton, Ontario, Canada, L8S 4M1

J. Martorell
Departamento d'Estructura i Constituents de la Materia, Facultat de Fisica, University of Barcelona, Barcelona 08028, Spain
(Received 3 December 1991)

The symmetrical two-dimensional quantum wire with two straight leads joined to an arbitrarily shaped interior cavity is studied with emphasis on the single-mode approximation. It is found that for both transmission and bound-state problems the solution is equivalent to that for an energy-dependent one-dimensional square well. Quantum wires with a circular bend, and with single and double right-angle bends, are examined as examples. We also indicate a possible way to detect bound states in a double bend based on the experimental setup of Wu *et al.* [Appl. Phys. Lett. **59**, 102 (1991)].

I. INTRODUCTION

Recent advances in nanometer-scale fabrication of GaAs heterosructures have attracted much attention to studies of mesoscopic systems.[1] Several authors have considered electron transport properties as well as electron bound states in various configurations.[2–23] Among the many devices studied, a large class may be characterized as being "uniform quantum wires connected to a cavity": electrons enter the device at one end of a straight lead, pass a region of a given geometric shape or potential field, and are transmitted into another lead or reflected back to the original lead. The properties of these devices can be determined numerically or, in some simple cases, analytically.[21,23] Nevertheless, it would be useful to have a simple physical picture that reproduces these results. In this paper, we study the case of a quite general quantum wire, requiring only the interior cavity shape and/or potential field to be symmetric with respect to the two leads; see Fig. 1. We first give a general formula to solve the problem exactly, based on the mode-matching method. We then propose a single-mode approximation to simplify the problem. This one-mode approximation usually gives rather good agreement with the exact result, and is sufficient to give a valid physical picture for energies less than the second excitation mode in the lead.[21] We shall prove that one can always find an effective one-dimensional square well which duplicates the behaviour of the device in the single-mode approximation, thereby providing a simple physical picture for a quantum wire operating at low energy. We will use this model to study circular bent wires and confirm the results of an earlier paper.[23] We will also apply the effective square-well model to the bound state of an L-shape wire. Finally we will present a detailed study of the bound states of multibend wires. In this case too the model proposed is very useful to interpret physical properties of such quantum wires.

II. GENERAL MODE-MATCHING FORMALISM FOR A SYMMETRICAL QUANTUM WIRE

The device we consider here is shown in Fig. 1. It has two straight leads of width d attached to a reflection-symmetric internal part of an otherwise arbitrary shape. Without loss of generality, we assume that the potential in the leads is uniform in the longitudinal direction. If this were not the case, one can always repartition the internal part and the leads so that the variable-potential part is excluded from the leads. In general, the potential in the leads in the transverse direction need not be constant. The transverse modes are then obtained by solving a one-dimensional eigenvalue problem. Let the solutions be $\phi_n(y)$ with eigenvalues ε_n. We also denote the lines dividing the leads from the internal region as σ_1 and σ_2. When in boldface these symbols are unit normal vectors pointing outward, as shown in Fig. 1. The solution in the leads can be expanded as

$$\Psi_\Gamma = \sum_n (C_{\Gamma,n} e^{i\alpha_n x} + \bar{C}_{\Gamma,n} e^{-i\alpha_n x})\phi_n(y) \quad , \tag{1}$$

where $\Gamma = 1, 2$ distinguishes the two leads, and

$$\alpha_n = \sqrt{E - \varepsilon_n} \tag{2}$$

is the longitudinal wave number associated with the transverse mode n. We express energies in units of $\hbar^2/2m^*$.

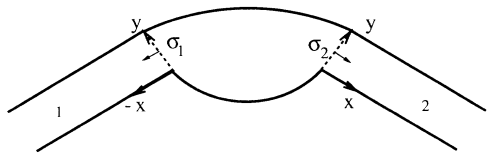

FIG. 1. Symmetrical two-dimensional quantum wire.

In the internal region, we define auxiliary wave functions χ_{n0} and χ_{0n} as those satisfying the original Schrödinger equation with the boundary conditions

$$\chi_{n0}|_{\sigma_1} = \chi_{0n}|_{\sigma_2} = \phi_n(y) \quad , \tag{3}$$

$$\chi_{0n}|_{\sigma_1} = \chi_{n0}|_{\sigma_2} = 0 \quad . \tag{4}$$

The actual wave function in the interior region is expanded in terms of these functions. By imposing continuity of the wave function at the boundaries, we have

$$\Psi = \sum_n (C_{1n}^+ \chi_{n0} + C_{2n}^+ \chi_{0n}) \quad , \tag{5}$$

where

$$C_{\Gamma,n}^{\pm} \equiv C_{\Gamma,n} \pm \bar{C}_{\Gamma,n} \quad . \tag{6}$$

Continuity for the wave function derivative yields

$$\sum_n C_{1n}^- i\alpha_n \phi_n(y) = -\sum_n [C_{1n}^+ (\nabla\chi_{n0}\cdot\boldsymbol{\sigma}_1) + C_{2n}^+ (\nabla\chi_{0n}\cdot\boldsymbol{\sigma}_1)] \quad , \tag{7}$$

and

$$\sum_n C_{2n}^- i\alpha_n \phi_n(y) = \sum_n [C_{1n}^+ (\nabla\chi_{n0}\cdot\boldsymbol{\sigma}_2) + C_{2n}^+ (\nabla\chi_{0n}\cdot\boldsymbol{\sigma}_2)] \quad . \tag{8}$$

Due to the assumed symmetry,

$$\nabla\chi_{n0}\cdot\boldsymbol{\sigma}_1 = \nabla\chi_{0n}\cdot\boldsymbol{\sigma}_2 \quad , \tag{9}$$

$$\nabla\chi_{n0}\cdot\boldsymbol{\sigma}_2 = \nabla\chi_{0n}\cdot\boldsymbol{\sigma}_1 \quad . \tag{10}$$

Taking this into account and using the orthogonality of the transverse mode wave functions, we have

$$i\alpha C_1^- = AC_2^+ - BC_1^+ \quad , \tag{11}$$

$$i\alpha C_2^- = BC_2^+ - AC_1^+ \quad , \tag{12}$$

where α is a diagonal matrix with elements α_n, $C_\Gamma^{\pm}$ are one-column matrices with elements $C_{\Gamma,n}^{\pm}$, and A, B are the square matrices :

$$A_{nn'} = -\int_0^d \phi_n(y)(\nabla\chi_{0n'}\cdot\boldsymbol{\sigma}_1)dy \quad , \tag{13}$$

$$B_{nn'} = \int_0^d \phi_n(y)(\nabla\chi_{0n'}\cdot\boldsymbol{\sigma}_2)dy \quad . \tag{14}$$

Equations (11) and (12) are the two basic relations resulting from mode matching; $C_\Gamma^{\pm}$ represent wave modes in the two leads, and the matrices A,B represent the propagation in the internal cavity which transforms and mixes the modes in the leads. In simple cases, ϕ_n, χ_{n0}, and χ_{0n} may be written analytically.[22] A common assumption is to give the leads infinitely high walls, and constant potential inside; then $\phi_n(y) = \sqrt{2/d}\sin(n\pi y/d)$.

For both the transmission and bound-state problems, there should be no backward-going wave in the exit lead. Let this be lead 2, then $\bar{C}_2 = 0$. This implies $C_2^+ = C_2^- = C_2$, and therefore

$$\begin{pmatrix} A & -(B-i\alpha) \\ (B-i\alpha) & -A \end{pmatrix} \begin{pmatrix} C_2 \\ \bar{C}_1 \end{pmatrix} = \begin{pmatrix} (B+i\alpha)C_1 \\ AC_1 \end{pmatrix} \quad . \tag{15}$$

For the transmission problem, C_1 specifies the incoming wave, and the problem reduces to solving a set of linear equations. For a bound state, $C_1 = 0$, and the problem is then to find a nontrivial solution to the homogeneous form of the above equations.

If instead of the single-cell cavity shown in Fig. 1 the device is actually made of several serially connected parts, propagation across each cell is also given by Eqs. (11) and (12). It is then convenient to rewrite them in the transfer-matrix form

$$\begin{pmatrix} C_1^+ \\ C_1^- \end{pmatrix} = \begin{pmatrix} A^{-1}B & -iA^{-1}\alpha \\ i\alpha^{-1}(BA^{-1}B - A) & \alpha^{-1}BA^{-1}\alpha \end{pmatrix} \begin{pmatrix} C_2^+ \\ C_2^- \end{pmatrix} . \tag{16}$$

Note that this is exactly the same as Eq.(40) in Ref. 22, as the T-shape cavity is just a special case of the cells that we are considering. Since Eq.(16) applies also to any cell of a serially connected device, the equivalence to be shown below of this transfer matrix to that of an effective one-dimensional square well will also hold for each component of a multicell device. Thus one may view a serially connected device at low energy as equivalent to a series of one-dimensional square wells. All the structure associated with Bloch waves should then be found for these systems, as discussed by Kouwenhoven *et al.*[10]

III. THE SINGLE-MODE APPROXIMATION AND EFFECTIVE ONE-DIMENSIONAL SQUARE WELL

When the energy of the incoming electron is below that of the second transverse excitation mode, there will be at most one open mode in the external channels. In principle, even in this situation, one still needs to deal with all the closed channels (for which α_n is imaginary). However, these closed channel components decrease exponentially as one goes from the interior of the device into the leads, which makes their effect small. The single-mode approximation therefore consists in truncating all matrices which appear in Eqs. (16) into 1×1 matrices, so that A and B become numbers and commute with each other. Then

$$\begin{pmatrix} C_1^+ \\ C_1^- \end{pmatrix} = \begin{pmatrix} B/A & -i\alpha/A \\ -i(A - B^2/A)/\alpha & B/A \end{pmatrix} \begin{pmatrix} C_2^+ \\ C_2^- \end{pmatrix} = \begin{pmatrix} B/A & -i\frac{\sqrt{A^2-B^2}}{A}\frac{\alpha}{\sqrt{A^2-B^2}} \\ -i\frac{\sqrt{A^2-B^2}}{A}\frac{\sqrt{A^2-B^2}}{\alpha} & B/A \end{pmatrix} \begin{pmatrix} C_2^+ \\ C_2^- \end{pmatrix} . \tag{17}$$

Furthermore, making the identifications

$$\gamma = \sqrt{A^2 - B^2} \tag{18}$$

and

$$\cos(\gamma w) = \frac{B}{A} \quad , \tag{19}$$

the transfer matrix in Eq. (17) which relates the input wave to the output wave takes the form

$$\begin{pmatrix} \cos(\gamma w) & -i\sin(\gamma w)\alpha/\gamma \\ -i\sin(\gamma w)\gamma/\alpha & \cos(\gamma w) \end{pmatrix}, \tag{20}$$

which is identical to that for a one-dimensional square well,[24] with γ and α being the wave numbers inside and outside the well, respectively, and w being the width of the well. The depth of the well is

$$\begin{aligned} V &= \gamma^2 - \alpha^2 \\ &= A^2 - B^2 - E + \varepsilon_1 \end{aligned} \tag{21}$$

and its width is fixed by Eq.(19). We have therefore shown that in the single-mode approximation, the transfer matrix for any symmetrical quantum wire is identical to that of an effective one-dimensional square well . Although the energy dependence of the depth and the width of the square well is a complication, this equivalence is nevertheless useful for the following reasons.

(i) First of all, it provides a clear physical picture of how the device operates at low energy, which has not been stated explicitly to date.

(ii) For some devices, simple formulas can be obtained for the effective potential depth and width in the energy region of interest, and thus provide useful practical information. We give examples in the next sections.

(iii) For bound states, the energy can be predetermined in a certain energy range, usually extremely close to the first transverse mode energy, and then the effective square well can be used to determine the bound-state energy. We give examples in what follows.

(iv) For devices consisting of serially connected parts, this effective square potential picture provides a simple intuitive means for finding qualitative features of the entire device.

It is interesting to ask whether an energy-independent local effective potential could be constructed to reproduce the transmission and bound-state properties. This is surely possible by a variant of the Gel'fand-Levitan[25] or Marchenko[26] constructions which are applied to three-dimensional scattering problems. Chadan and Sabatier discuss such a construction.[27]

IV. EFFECTIVE SQUARE WELL FOR A QUANTUM WIRE WITH A CIRCULAR BEND

Quantum wires of uniform width with a circular bend have been studied recently by Sols[17] and Lent[18] by means of detailed numerical calculations. We have shown in a recent paper[23] that such a system can be well understood by an effective square-well model with width $(R + d/2)\theta$ and depth $1/[4(R+d/2)^2]$, where R is the inner radius of the bend, d is the width of the wire, and θ is the bending angle. With the method discussed in the preceding section, we can put this effective square well on more solid ground.

For the straight leads, $\phi_n = \sqrt{2/d}\sin(\pi n y/d)$. We use polar coordinates (r, ϕ) for the bend, $R \le r \le R + d$, $0 \le \phi \le \theta$. After separating variables, the angle dependence will be $\exp(\pm im\phi)$ while the radial part satisfies Bessel's equation. In general, it is a linear combination of Bessel functions of the first kind, $J_m(kr)$, and the second kind, $N_m(kr)$, where $k = \sqrt{E}$. The hard wall assumption requires that the radial wave vanishes at $r = R$ and $R + d$. The first condition is automatically satisfied by the radial function

$$Z_m(kr) \equiv \mathcal{N}_m[N_m(kR)J_m(kr) - J_m(kR)N_m(kr)] \quad , \tag{22}$$

where $\mathcal{N}_m$ is a normalization constant. The second condition

$$Z_m[k(R + d)] = 0 \tag{23}$$

quantizes the angular wave mode m. Let us denote these m values as m_j. The first m value, m_1, corresponds to a radial wave function with no node in the interval $R < r < R + d$, i.e., a half standing wave. The next mode has one node and so on. Since the total energy is fixed, as we move to higher radial excitation modes, m_j will become complex. By choosing $\mathcal{N}_m$ appropriately, the set of Z functions for fixed k become an ortho-normal set with the weighting function $1/r$:

$$\int_R^{R+d} Z_{m_j} Z_{m_{j'}} \frac{1}{r} dr = \delta_{j,j'}. \tag{24}$$

The auxiliary functions $\chi_{0n}(\phi, r)$ satisfy boundary conditions:

$$\chi_{0n}(\phi = 0, r = R + y) = 0, \tag{25}$$

$$\chi_{0n}(\phi = \theta, r = R + y) = \sqrt{2/d}\sin(\pi n y/d), \tag{26}$$

and are expanded on the set of functions

$$\exp(\pm im_j\phi)Z_{m_j}(kr), j = 1, ...,$$

giving

$$\chi_{0n} = \sum_j \frac{\sin(m_j\phi)}{\sin(m_j\theta)} I_{nj} Z_{m_j}(kr) \quad , \tag{27}$$

where

$$I_{nj} = \sqrt{\frac{2}{d}} \int_R^{R+d} \sin[n\pi(r - R)/d] Z_{m_j}(kr) \frac{1}{r} dr. \tag{28}$$

It follows that the matrices A and B are

$$A_{nn'} = \sum_j \frac{m_j}{\sin(m_j\theta)} I_{nj} I_{n'j}, \tag{29}$$

$$B_{nn'} = \sum_j m_j \cot(m_j\theta) I_{nj} I_{n'j}. \tag{30}$$

Note that they are symmetric and real.

Once A and B are known, the transmission and reflection coefficients can be determined by solving Eq. (15). Further simplification is made by taking only one term in Eqs. (29) and (30). A comparison with the full scale calculation shows that this is a very good approximation. The agreement is essentially like that shown in Figs. 1 and 2 in Ref. 23. With this further approximation,

$$A \equiv A_{11} = \frac{m}{\sin(m\theta)} I^2 \quad (m \equiv m_1, I \equiv I_{11}) \quad , \tag{31}$$

$$B \equiv B_{11} = m\cot(m\theta) I^2 . \tag{32}$$

Thus

$$\gamma = mI^2, \quad w = \frac{m\theta}{\gamma} = \frac{\theta}{I^2} \quad . \tag{33}$$

The quantity I^2 has dimension of $(\text{length})^{-1}$ and its meaning is best revealed in the large R limit. When R is large, the Bessel function takes its asymptotic form. In this region,

$$Z_m(kr) \propto \frac{1}{\sqrt{r}} \sin\left[ky + \frac{4m^2-1}{8k}\left(\frac{1}{R+y} - \frac{1}{R}\right)\right] \tag{34}$$

and keeping only terms of lowest order in y/R,

$$Z_m(kr) \propto \frac{1}{\sqrt{r}} \sin\left(k - \frac{4m^2-1}{8kR^2}\right) y \approx \frac{1}{\sqrt{r}} \sin\left(\frac{\pi y}{d}\right) \quad . \tag{35}$$

Here we have applied the boundary condition at the outer edge of the curved wire, Eq.(23), and we see that for the lowest mode,

$$m^2 = \tfrac{1}{4} + 2kR^2\left(k - \frac{\pi}{d}\right) \quad . \tag{36}$$

Substituting this into Eq. (28) and taking care of a normalization constant gives

$$I^2 = \frac{2}{d} \frac{\left(\int_0^d \sin^2(\pi y/d)(R+y)^{-3/2} dy\right)^2}{\int_0^d \sin^2(\pi y/d)(R+y)^{-2} dy} \approx \frac{1}{R + d/2} . \tag{37}$$

Therefore we define

$$\bar{R} = 1/I^2 \tag{38}$$

as an effective radius, for which the value $R + d/2$ was used in Ref. 23. In terms of $\bar{R}$, Eq. (33) gives

$$\gamma = m/\bar{R}, \quad w = \bar{R}\theta. \tag{39}$$

Thus $\bar{R}$ directly determines the width of the square well, which is just the arc length of radius $\bar{R}$. In Fig. 2 we show the effective radius computed from Eqs. (28) and (38), using the exact Z_m. These results confirm that in general $\bar{R}$ is quite close to $R + d/2$, except for the smallest values of $R < d/2$.

From Eqs.(21) and (31)–(33), the depth of the effective square well is found to be

$$V = \frac{m^2}{\bar{R}^2} - k^2 + \left(\frac{\pi}{d}\right)^2 . \tag{40}$$

The numerical results are shown in Fig. 3. The bound state is located below $k = \pi/d$ but extremely close to it. The region where transmission is practically not 1 is just above $k = \pi/d$ and does not extend very far. Hence the depth of the well in this region is of great practical interest. It does not vary much. The analytical expression at $k = \pi/d$ can be found easily: from Eq.(36), $m^2 = \frac{1}{4}$, and

$$V|_{k=\pi/d} = \frac{1}{4\bar{R}^2} . \tag{41}$$

This is the potential used in Ref. 23. We conclude that

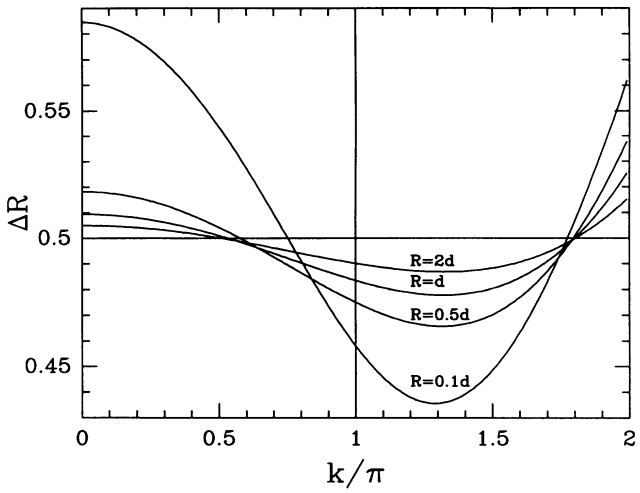

FIG. 2. The difference between the effective radius of a circular-bend wire and the inner radius, $\Delta R = \bar{R} - R$, in units of d.

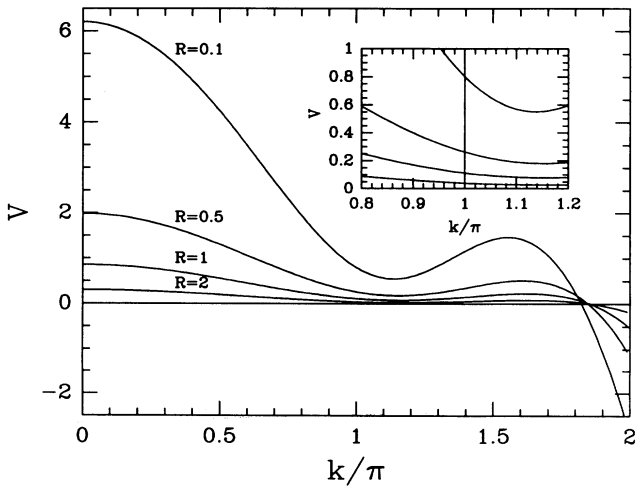

FIG. 3. The effective square-well depth for circular-bend wires for various inner radii R. Inset is a magnification around $k \approx \pi$.

the properties of a circular-bend wire in the low-energy region can be well understood with an effective square well of width $w = \bar{R}\theta$ and depth $1/(4\bar{R}^2)$.

V. EFFECTIVE SQUARE WELL FOR THE L-SHAPE WIRE

The L-shape wire was studied by Exner, Seba, and Stovicek[15] and by us.[21] Alternative treatments can be found, for example, in Weisshaar *et al.*,[7] Schult, Ravenhall, and Wyld,[13] and Wu *et al.*[20] Figure 4 shows the shape of the device and the coordinate systems used below.

The transverse mode wave functions in the leads are $\sqrt{(2/d)}\sin(n\pi y_1/d)$ for lead 1 and $\sqrt{(2/d)}\sin(n\pi y_2/d)$ for lead 2. It is easy to find the function χ_{0n}:

$$\chi_{0n} = \sqrt{\frac{2}{d}}\sin\left(\frac{n\pi Y}{d}\right)\frac{\sin(\alpha_n X)}{\sin(\alpha_n d)}, \tag{42}$$

and it follows that

$$\nabla\chi_{0n}\cdot\boldsymbol{\sigma}_1 = \sqrt{\frac{2}{d}}\frac{n\pi}{d}(-1)^n\frac{\sin(\alpha_n X)}{\sin(\alpha_n d)} \tag{43}$$

and

$$\nabla\chi_{0n}\cdot\boldsymbol{\sigma}_2 = \sqrt{\frac{2}{d}}\alpha_n\sin\left(\frac{n\pi Y}{d}\right)\cot(\alpha_n d) \quad . \tag{44}$$

Therefore the matrices A and B are explicitly

$$A_{nn'} = \frac{2nn'\pi^2(-1)^{n+n'}}{d[(n\pi)^2-(\alpha_{n'}d)^2]}, \tag{45}$$

$$B_{nn'} = \alpha_n\cot(\alpha_n d)\delta_{nn'} \quad . \tag{46}$$

In the one-mode approximation,

$$A = \frac{2\pi^2}{d[\pi^2-(\alpha d)^2]}, \tag{47}$$

$$B = \alpha\cot(\alpha d). \tag{48}$$

Since A and B are known, the parameters of the effective square well can be calculated in a straightforward way. From these, and without further approximations, the analytic expression given for the transmission coefficient in Ref. 21, Eqs. (21)–(23), can be easily obtained. By looking at fig. 1 of that reference it can be checked that for this case also, the one-mode approximation is very good for energies below the second transverse mode threshold. Similarly, for the bound state from table 1 of Ref. 21 one can see that the approximation is rather accurate. However, we are particularly interested in the limit when α is small. Neglecting second-order terms in α in Eqs.(47) and (48) one finds $A = 2/d$ and $B = 1/d$. Thus $\gamma = \sqrt{A^2-B^2} = \sqrt{3}/d$, $\cos(\gamma w) = B/A = \frac{1}{2}$, $\gamma w = \pi/3$. This leads to

$$w = \frac{\pi}{3\sqrt{3}}d \tag{49}$$

and

$$V = \frac{3}{d^2}. \tag{50}$$

Using this effective square well we find the bound-state energy to be $0.938\varepsilon_1$, while the exact result is at $0.929\varepsilon_1$.[15,21]

VI. BOUND STATES OF WIRES WITH MULTIPLE RIGHT-ANGLE BENDS

There are two kinds of double right-angle bends, as shown in Figs. 5(a) and 5(b). One has a U shape and the other a step shape. A special case of the U-shape double bend has been discussed by Bar-Touv and Avishai.[28] Weisshaar *et al.*[7] studied the step shape double bend using a mode-matching method, and the paper by Wu *et al.*[20] reports on an experimental determination of the conductance for the step shape.

We have made exact two-dimensional calculations for the bound states of the U and step shapes. This was done by applying Eqs.(11) and (12) to each single bend and retaining enough modes (about 25) throughout the calculation. The binding energies are shown in Fig. 6, as a function of the distance between the bends. A double bend can be viewed as two interacting single bends. When the interbend distance (L) is large, the two single bends almost decouple from each other and we find two degenerate bound states, one state with even symmetry and the other with odd symmetry. The wave function

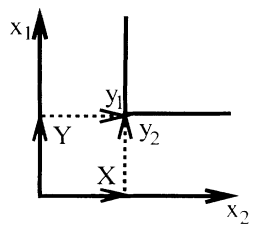

FIG. 4. An L-shaped wire of width d with coordinates in three regions. (x_1, y_1) for lead 1, (x_2, y_2) for lead 2, and (X, Y) for the internal region.

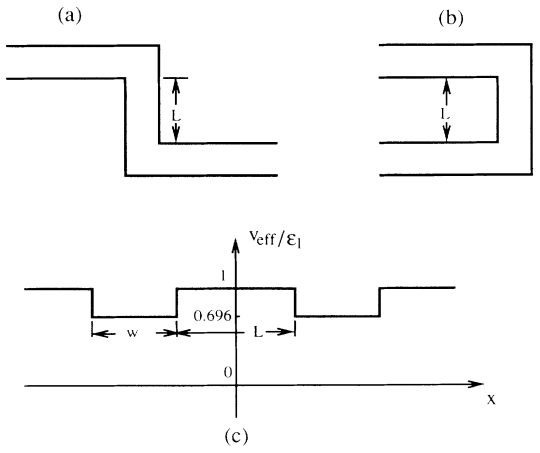

FIG. 5. (a) A one-step double bend of width d and interbend distance L. (b) A U-shape double bend. (c) The effective one-dimensional potential of a double square-well model for both types of double bend.

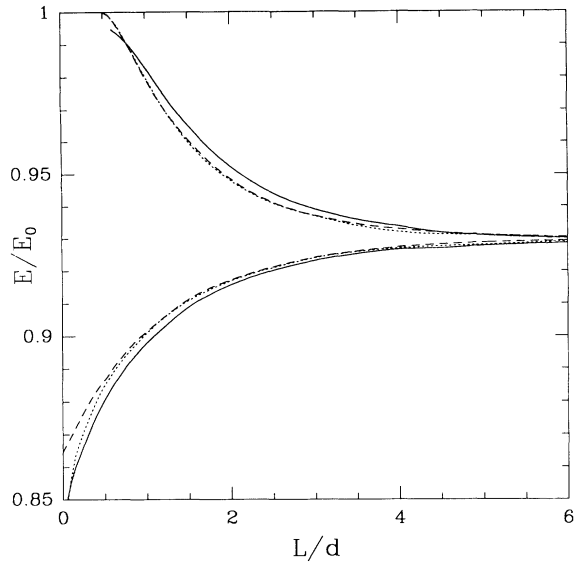

FIG. 6. Bound states of a double bend as a function of the interbend distance. Solid line: energies given by the double square-well model, shifted down by $0.009\varepsilon_1$. Dotted and dashed lines: Exact energies for U-shape and one-step double bends, respectively.

of the odd-symmetry state vanishes at the midpoint of the connecting wire. When L is shortened, confinement pushes the energy of the odd state up while lowering that of the even state. This is exactly the same behavior as obtained for two one-dimensional square wells separated a certain distance.

We have also calculated the bound-state energy of the double bend using the model of two one-dimensional square wells . The depth and the width of each well are taken from the preceding section, Eqs. (49) and (50); see Fig. 5(c). In the single-mode approximation, there is no difference between the U shape and the step double bend, and indeed we see in Fig. 6 that the low-energy behaviors of the exact calculations for the two shapes are similar. In order to emphasize the special features of the double bend, we have shifted the double square well results down by $0.009\varepsilon_1$, so that the three curves approach the same asymptotic value. We see that the agreement is excellent. The U-shape energies are almost identical to those of the step shape except at very small L values. This can be understood from a classical picture. When L is very small, an electron can be transmitted more easily through the step shape than through the U shape.

Two additional features are worthy of mention. One is that the odd-symmetry state is bound only when L is long enough, greater than about $0.5d$. Recall that the wave function must vanish at the midpoint, thus it has to drop from a finite value at the edge of the bend to zero within a distance $0.25d$. Another feature concerns the $L < 0$ case. By definition, negative values of L are only possible for the step shape. When $L = -d$, the device is just a straight wire, with no bound state. As L decreases from 0 to $-d$, the even-symmetry state rises from its minimum value of $\approx 0.865\varepsilon_1$ to 1. Thus by using a double bend, one can double the binding energy compared to that for a single bend. That the minimum bound-state energy is obtained when $L = 0$ is also predicted by the double square-well model: after the two wells start touching, a further reduction in the interwell distance decreases the total width of the merged well and thus pushes the bound state up. This property has interesting consequences for multistep devices as we will discuss in what follows.

Figure 7 is a sketch of three possible types of multistep shapes. We shall call the one with $L = 0$ the proper-step staircase, the $L < 0$ shape the small-step staircase, and the $L > 0$ shape the large-step staircase. The argument given for the double bend indicates that the proper-step staircase should have the lowest bound state. Its energy can be estimated from Eqs. (49) and (50): the equivalent square well has depth $3/d^2$ and width $n_b\pi/(3\sqrt{3})d$, where n_b stands for the number of bends in the staircase. Therefore in that model the bound state energies are

n_b	1	2	3	4	5	6	...	∞
e/ε_1	0.938	0.856	0.804	0.772	0.752	0.730	...	0.696.

(51)

When n_b approaches infinity, the bound state drops towards the bottom of the square well: $(1 - 3/\pi^2)\varepsilon_1$. This shows that the energy of the bottom of the effective square well is just the minimum energy for an electron wave to be able to propagate in a proper-step staircase quantum wire.

We will now discuss possible ways to detect double-bend (or multibend) bound states in current experiments. Wu *et al.* have measured the conductance of a multistep double-bend wire. We model their device as shown in Fig. 8. Electrons are excluded from the blackened areas by applying a negative potential to the gates. By varying the

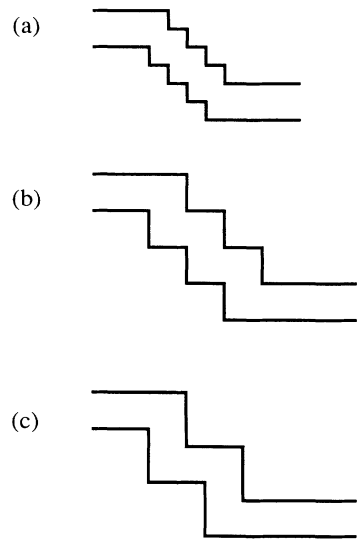

FIG. 7. Multistep quantum wires. (a) Small-step staircase (8 bends), (b) proper-step staircase (6 bends), and (c) large-step staircase (4 bends).

applied potential, the width of the double bend can be changed. The double-bend wire is connected to two reservoirs, which are much wider than the leads themselves. Because of these wider leads, the device can be operated at an energy lower than the first transverse mode energy of the double bend. When the electron energy is equal to one of the bound-state energies, we expect to see a resonant tunneling peak in the conductance. Berggren and Zhen[16] have discussed a similar situation for cross- and T-shaped devices. In the measurement of Wu *et al.* the L and L_l values are very large compared to the width d (see Fig. 8), thus the predicted resonant tunneling peaks are very narrow and in fact cannot be seen in the data. (This is why they attribute the two peaks seen below the first mode to impurity scattering.)

We have made a calculation for the device shown in Fig. 8. We assume that the two external leads are very wide. (A width of $20d$ is used. As a test of convergence in regard to this width, we found that there is little difference if we use $10d$ instead.) We have studied the conductance for energies close to the threshold $\varepsilon_1 = (\pi/d)^2$. Thus we may greatly simplify our calculation by simply using a double square well to model the double bend. For simplicity of discussion, we model the actual experiment by assuming that when the potential applied to the gates is varied, the Fermi energy remains constant and the effective electron blocking area is changed in such a way that any extension or reduction is equal in both the x and y directions. Thus when d is changed by δd, i.e., $d \to d + \delta d$, L and L_l will be changed to $L \to L - \delta d$, $L_l \to L_l - \delta d$. For a given energy we denote the critical value of d for which the double bend opens for the first mode to be $d_1 = \pi/\sqrt{e}$.

Figure 9 plots the conductance versus the width d. We have used L and L_l values comparable to d. The solid curve is for the case $L = L_l = (2.205d_1 - d)$. There are two peaks below $d = d_1$. The first one is at $d = 0.954d_1$, and corresponds to $L/d = 1.311$. In terms of $(\pi/d)^2$, the electron energy is at 0.910. On the other hand, at this ratio, the dashed line in Fig. 6 shows (for the one-step double bend) that the even-symmetry bound-state energy is 0.908. Therefore we identify this peak as resonant tunneling via the even bound state. The next peak is at $d = 0.987d_1$, giving $e = 0.973(\pi/d)^2$ and $L/d = 1.235$.

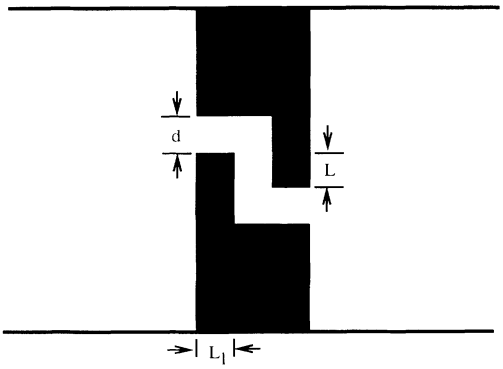

FIG. 8. Illustration of proposed device to detect double-bend bound states.

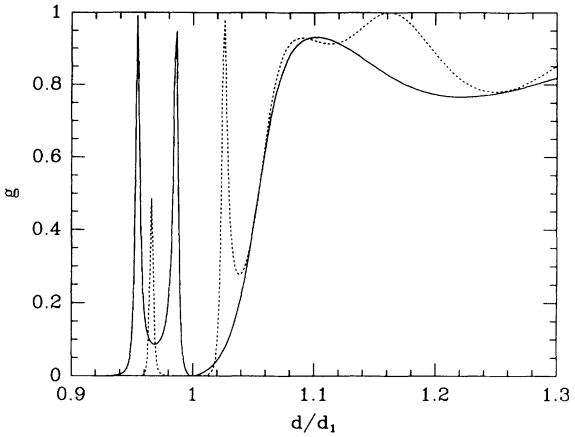

FIG. 9. Conductance versus double bend width of the device shown in Fig. 8. The conductance is in units of $2e^2/h$. The solid curve corresponds to $L = L_l = 2.205d_1 - d$ while the dotted curve corresponds to $L = 5.513d_1 - d$ and $L_l = 2.205d_1 - d$. $d_1 = \pi/\sqrt{e}$ is the width of a long straight wire for which the first propagating channel would be open at energy e.

Figure 6 shows the odd bound state at $0.970(\pi/d)^2$. Thus this peak is due to resonant tunnelling through the odd bound state. The dotted curve is for $L = 5.513d_1 - d$ and $L_l = 2.205d_1 - d$. The relatively large L value results in almost degenerate even and odd bound states, thus only one degenerate peak is seen d_1. This peak is located at $d = 0.966d_1$, with $e = 0.933(\pi/d)^2$ and $L/d = 4.708$. Figure 6 gives the even state at $0.928(\pi/d)^2$ and odd state at $0.932(\pi/d)^2$. These binding energies will be reduced in a real wire which has only finite walls.

VII. CONCLUSION

In this paper we have given a general mode-matching formula for a symmetric quantum wire. By use of the single mode approximation, we have found that the device in the low-energy region can be understood by means of an effective one-dimensional square well. The one-dimensional nature of the wire at energies below the second transverse mode has been recognized widely, but we provide a quantitative description. We have discussed a possible way to detect the bound state in a multi-bend wire. We have identified the depth of the effective well for a right-angle bend as the reduction in minimum energy for propagation in a long corrugated wire as opposed to a straight wire. This corroborates the similar situation for the circular-bend wire.[17]

ACKNOWLEDGMENTS

We are grateful to NSERC Canada for continuing support under operating grant A-3198 (D.W.L.S. and H.W.). The work of J.M. was partially supported under grant PB-87-0311 from DGICYT Spain. In addition, D.W.L.S. is grateful to the Spanish Ministry of Science and Education (DGICYT) for support at the University of Barcelona, where some of this work was performed.

[1] See Phys. Today **43** (2), 22 (1990).
[2] S. Datta, Superlatt. Microstruct. **6**, 83 (1989).
[3] S. Datta, in *Physics of Quantum Electron Devices*, edited by F. Cappasso, Springer Series in Electronics and Photonics Vol. 28 (Springer-Verlag, Berlin, 1990), pp. 321–352.
[4] F. Sols, M. Macucci, U. Ravaioli, and K. Hess, Appl. Phys. Lett. **54**, 350 (1989).
[5] F. Sols, M. Macucci, U. Ravaioli, and K. Hess, J. Appl. Phys. **66**, 3892 (1989).
[6] A. Szafer and A. D. Stone, Phys. Rev. Lett. **62**, 300 (1989).
[7] A. Weisshaar, J. Lary, S. M. Goodnick, and V. K. Tripathi, Appl. Phys. Lett. **55**, 2114 (1989).
[8] Y. Avishai and Y. B. Band, Phys. Rev. B **41**, 3253 (1990); Y. Avishai, M. Kaveh, and Y.B. Band, *ibid.* **42**, 5867 (1990).
[9] C. G. Smith, M. Pepper, H. Ahmed, J. E. F. Frost, D. G. Hasko, R. Newbury, D.C. Peacock, D. A. Ritchie, and G. A. C. Jones, J. Phys. Condens. Matter **1**, 9035 (1989).
[10] L. P. van Kouwenhoven , F. W. J. Hekking, B. J. van Wees, C. J. P. M. Harmans, C. E. Timmering, and C. T. Foxon, Phys. Rev. Lett. **65**, 361 (1990).
[11] S.E. Ulloa, E.Castaño, and G. Kirczenow, Phys. Rev. B **41**, 12 350 (1990).
[12] E.Castaño and G.Kirczenow, Solid State Commun. **70**, 801 (1989).
[13] R.L. Schult, D.G. Ravenhall, and H.W. Wyld, Phys. Rev. B **39**, 5476 (1989).
[14] D.G. Ravenhall, H.W. Wyld, and R.L. Schult, Phys. Rev. Lett. **62**, 1780 (1989).
[15] P. Exner, P. Seba, and P. Stovicek, Czech. J. Phys. B **39**, 1181 (1989).
[16] K.-F. Berggren and Zhen-li Ji, Superlatt. Microstruct. **8**, 59 (1990); Phys. Rev. B **43**, 4760 (1991).
[17] F. Sols and M. Macucci, Phys. Rev. B **41**, 11 887 (1990).
[18] C. S. Lent, Appl. Phys. Lett. **56**, 2554 (1990).
[19] J. A. Brum, Phys. Rev. B **43**, 12 082 (1991).
[20] J. C. Wu, M. N. Wybourne, W. Yindeepol, A. Weisshaar, and S. M. Goodnick, Appl. Phys. Lett. **59**, 102 (1991).
[21] J. Martorell, S. Klarsfeld, D. W. L. Sprung, and Hua Wu, Solid State Commun. **78**, 13 (1991).
[22] Hua Wu, D. W. L. Sprung, J. Martorell, and S. Klarsfeld, Phys. Rev. B **44**, 6351 (1991).
[23] D. W. L. Sprung, Hua Wu, and J. Martorell, J. Appl. Phys. **71**, 515 (1992).
[24] E. Merzbacher, *Quantum Mechanics*, 2nd ed. (Wiley, New York, 1970), Eq. 6.49.
[25] I. M. Gel'fand and B. M. Levitan, Izv. Akad. Nauk SSSR, Ser. Math. **15**, 309 (1951); Am. Math. Soc. Transl. Ser. 2, **1**, 253 (1955).
[26] V. A. Marchenko, Dokl. Akad. Nauk SSSR **72**, 457 (1950); see also Math. Rev. **12**, 183 (1951); V. de Alfaro and T. Regge, *Potential Scattering* (North-Holland, Amsterdam, 1965), p. 150.
[27] K. Chadan and P. C. Sabatier, *Inverse Problems in Quantum Scattering Theory* (Springer-Verlag, New York, 1989).
[28] J. Bar-Touv and Y. Avishai, Phys. Rev. B **42**, 11 496 (1990).